Computers and Electronics in Agriculture 157 (2019) 509–517

Contents lists available at ScienceDirect

Computers and Electronics in Agriculture

journal homepage: www.elsevier.com/locate/compag

Original papers

Detecting fruit surface wetness using a custom-built low-resolution thermal-RGB imager

Yasin Osroosh*, R. Troy Peters

Irrigated Agriculture Research and Extension Center, Washington State University-Prosser, WA, United States

ARTICLE INFO

Keywords:
Sweet cherry
Cracking
Surface wetness
Thermal and RGB imagery
Wetness sensor

ABSTRACT

Sweet cherry fruit cracking caused by seasonal rains is a major source of crop loss in the U.S. Pacific Northwest region and around the globe. In-field monitoring of cherry fruit surface wetness and temperature is, therefore, very important in fruit loss management. To determine the feasibility of low-resolution thermal-RGB imagery for detecting sweet cherry surface wetness, an experiment was carried out in plots of Skeena and Selah cherry varieties with Y-trellised and vertical architecture, respectively, at the Roza Farm of Washington State University, Prosser, WA. To wet cherries, 5 mm of rain was applied by running a rain simulator for 4 min (1.25 mm min^{-1}) above canopies. Rainwater samples were collected using five rain gauges to quantify the applied amount of water. The in-field sensing setup included two custom-built thermal-RGB imagers, a micro-climate-measuring unit and two leaf wetness sensors. The imagers were installed at a height of 2.1 m above the ground surface and were about 20 cm from the target cherries. The leaf wetness sensors were next to the cherries in the field of view of the imagers. A custom computer vision algorithm was developed and used to identify leaves and cherries in thermal and RGB images and extract the surface temperatures. The relationship between raw and normalized surface temperature, and wetness level and duration was investigated. The applicability of normalized cherry surface and air temperature difference was also studied. The results revealed that low-resolution thermal-RGB imagery can be used for detecting cherry fruit wetness level and duration. There was also a high correlation between the surface temperature of leaves and cherry fruits during the wetness period suggesting the temperature of leaves as reliable surrogate for cherry surface wetness and temperature monitoring. By utilizing the proposed imagery-based system, decision aid tools may be developed for efficient rainwater removal to prevent fruit cracking.

1. Introduction

The surface wetness and temperature of fruit are important parameters in pre- and post-harvest crop loss management. Some varieties of fresh-market fruit, such as sweet cherry, tomatoes and grapes are sensitive to the presence of moisture on fruit surface (i.e. fruit surface wetness), which may lead to fruit cracking/splitting and loss of fresh-market values. For example, sweet cherry faces the challenge of crop loss up to 90% in some varieties due to fruit splitting/cracking from seasonal rains prior to harvest (Zhou et al., 2016). Sweet cherry fruit cracking caused by rainwater is a major source of financial loss to growers around the globe and especially in the pacific region of the United States. Timely removal of rainwater from fruit surface requires accurate and real-time monitoring of fruit wetness in the field as part of a crop loss management system. Surface wetness and duration are also used for monitoring, prediction and management of disease in high value crops (Sutton et al., 1984; Rowlandson et al., 2015). Previous evidence has shown that bacteria and fungi are closely related to the humidity and wetness of fruit and canopy, and can be used to determine critical times for chemical spray applications (Llorente et al., 2000; Peres and Timmer, 2006; Duttweiler et al., 2008). The surface humidity and temperature of diseased fruit may be different from that of healthy fruits. Quantification of fruit surface wetness and temperature could thus provide a promising way for monitoring and prediction of disease/pests in tree fruit crops.

Considering the difficulty involved in direct measurements of fruit surface wetness, leaf-shaped flat plate type sensors are currently being used as the main indirect methods of quantifying surface wetness (Sentelhas et al., 2007). This type of wetness sensor, however, has shown to be very unreliable. The principle behind wetness sensing is relating either the dielectric constant or resistance of a grid of copper wires printed on the substrate surface to the presence or absence of

* Corresponding author.
E-mail address: yosroosh@gmail.com (Y. Osroosh).

https://doi.org/10.1016/j.compag.2019.01.023
Received 21 November 2018; Received in revised form 17 January 2019; Accepted 20 January 2019

water. The wetness sensor sampling size is limited to the area of the sensor and in some cases, the sensor may not even detect any moisture due to its small size. Moreover, thermal properties and shape of current wetness sensors are very different from that of an actual fruit making them incompetent of mimicking fruits (Hatfield, 1982).

In recent years, thermal sensing has found its way into many applications in precision agriculture (Khanal et al., 2017). Field scale remote sensing based on infrared thermography is known to be capable of characterizing leaf wetness duration (Sankaran et al., 2010; Mahlein et al., 2012). Ramalingam et al. (2004) showed the feasibility of using a sensor array comprised of a multispectral imager and an infrared thermometer in detecting and quantifying leaf surface wetness in a greenhouse. They developed a spraying system based on information from the sensor array, which was able to detect and spray a dry spot within a canopy. Leaf surface wetness in the form of dew has proven to be detectable using ground-based radiometry (Pinter, 1986; Hornbuckle et al., 2006) and satellite imagery (Cosh et al., 2009). Heusinkveld et al. (2008) developed a remote optical wetness sensor for field applications, which scans the surface and analyzes resulting spectral reflectance at two wavebands. They reported that the sensor was able to detect both leaf surface wetness and internal water.

In a previous study, we harnessed the power of recent technological advancements in the area of thermal sensing and single-board computers to develop an inexpensive thermal-RGB imaging system (Osroosh et al., 2018). This system was later used for monitoring apple sunburn in two apple varieties (Chandel et al., 2018). In the present study, our main goal was to evaluate the same system for monitoring the level and duration of cherry fruit surface wetness. To the best of our knowledge, combined thermal and RGB imagery has not been used for monitoring surface wetness and duration especially for small fruit surface wetness monitoring. The specific objectives were to (i) use a fully automated thermal-RGB imagery-based data acquisition system for monitoring sweet cherry fruit surface under field conditions, (ii) develop image-processing and computer vision algorithms to extract cherry fruit surface temperature from acquired images, and (iii) relate fruit surface temperature and microclimate measurements to fruit surface wetness, and evaluate the performance of the system in detecting fruit surface wetness.

2. Materials and methods

2.1. Experimental field

A field experiment was carried out in plots of Skeena (Y-trellised) and Selah (vertical canopy architecture) cherry varieties at Washington State University Roza Farm near Prosser, WA (latitude: 46.38°N, longitude: 120.46°W, and elevation: 239 m above sea level). The experiment was conducted in the 2017 season at the fruit maturing stage of selected cultivars, two weeks prior to the commercial harvesting window.

2.2. Microclimate monitoring system

The microclimate information including wind velocity, air temperature and relative humidity were measured using an ATMOS 41® unit (METER Group Inc., Pullman, WA). The unit uses the SDI-12 communication protocol and provides twelve different microclimate parameters. The unit was installed at standard height of 1.5 m above the ground level. Two leaf wetness sensors (LWS, METER Group Inc., Pullman, WA) connected to a datalogger (CR6, Campbell Scientific, Logan, UT) were used to quantify wetness level and duration of tree canopies. To determine the wetness duration by observation, our team inspected the canopies and recorded the time cherries and leaves took to dry after a simulated rainfall event. LWSs were fixated to tree branches in the view of imagers (discussed later) at 45–60° zenith angle, to mimic real leaves (Zhou et al., 2017). Each treatment had one LWS wired to the same datalogger as the microclimate sensing unit. All sensors logged data at a rate of one sample per minute.

2.3. Rainfall simulation system

To simulate rain in the orchard, a portable rainfall simulation system previously developed by Zhou et al. (2016) was used in this study. The setup consisted of a pumping system (Model 1538, Hypro, New Brighton, MN, USA) that provides pressurized water to eight sets of nozzles (Model FCX80, Hypro, New Brighton, MN, USA), each with a flow rate of 1.3 L min^{-1} at 275 kPa. In our experiment, the pressure was adjusted to 200 kPa and water discharged from approximately 1.0 m above top of tree canopies. This provided a coverage area of approximately 13.7 m^2 (Kafle et al., 2016). The study aimed at applying 5 mm of rain by running the rain simulator for 4 min (1.25 mm min^{-1}). This rainfall level was selected based on the average daily rainfall at the experimental site in the months of June and July as suggested by Zhou et al. (2017). The rainfall was sampled using five manual rain gauges attached to trellis wires at various heights and locations as described in Kafle et al. (2016). The amount of rain was calculated by averaging the five measurements. A buffer distance of about 20 m was maintained between two adjacent treatments to reduce the chance of simulated rainfall interference.

2.4. Thermal-RGB imaging system and field data collection

In this study, we used a thermal-RGB imaging system previously developed by our group (Osroosh et al., 2018). The electronics and associated hardware of the imager mainly consisted of a Raspberry Pi 3 board (Raspberry Pi Foundation) and camera modules. The thermal module (FLIR Lepton® 2.5, FLIR Systems, Inc., Wilsonville, OR) was radiometric with an automatic shutter. It had a resolution of 80 (horizontal) × 60 (vertical) pixels, horizontal field of view (HFOV) of 51°, a reported accuracy of ± 5 °C, frame rate of 9 Hz, and a spectral response wavelength range of 8–14 μ. The RGB camera module (Pi Camera 2, Raspberry Pi Foundation) had a resolution of 3280 × 2464 pixels, HFOV of 62.2°, vertical field of view (VFOV) of 48.8°. The imager could capture images automatically at specified time intervals or manually take snapshots. Captured images were processed and stored on a secured digital card. Thermal and RGB images were recorded at each timestamp in binary and JPG formats, respectively.

The field setup can be seen in Fig. 1. The setup included two thermal-RGB images calibrated in the lab using a blackbody calibrator (BB701, Omega Engineering, Inc., Stamford, CT), a microclimate sensing unit and two leaf wetness sensors. The imagers were installed at a height of about 2.1 m from the ground surface. They were about 20 cm from the cherries and leaves pointing at them at a 90° zenith angle. The microclimate sensing unit was installed at a height of 1.5 m and about 50 cm from the trees next to the imagers. The leaf wetness sensors were next to the cherries in the field of view of the imagers. Collected thermal and RGB images were used to relate temperature change to canopy and fruit surface wetness level. Measurements were taken at three locations using two imagers per location making a total of six replications (Fig. 2). Data collection at each location, continued until observed canopies including leaves and cherries were deemed to be dry.

2.5. Data and image analysis

Included in the field of view of an imager were cherries, canopy leaves, sky, and artificial objects such as sensors. A custom algorithm was developed to automatically detect these components in an RGB image using Matlab (2017Ra, MathWorks, Natick, MA), and to extract the surface temperature (average) of cherry leaves and fruits. A simplified flowchart of the image-processing and computer vision algorithm is depicted in Fig. 3. The algorithm took RGB and thermal images, cropped, resized and overlapped them, and created binary masks. Thermal images were converted to a matrix (80 × 60) of

Fig. 1. Field installation of the imaging system and measurements in the sweet cherry plots: rain simulator (a), thermal-RGB imagers and microclimate-measuring unit (b, c, d).

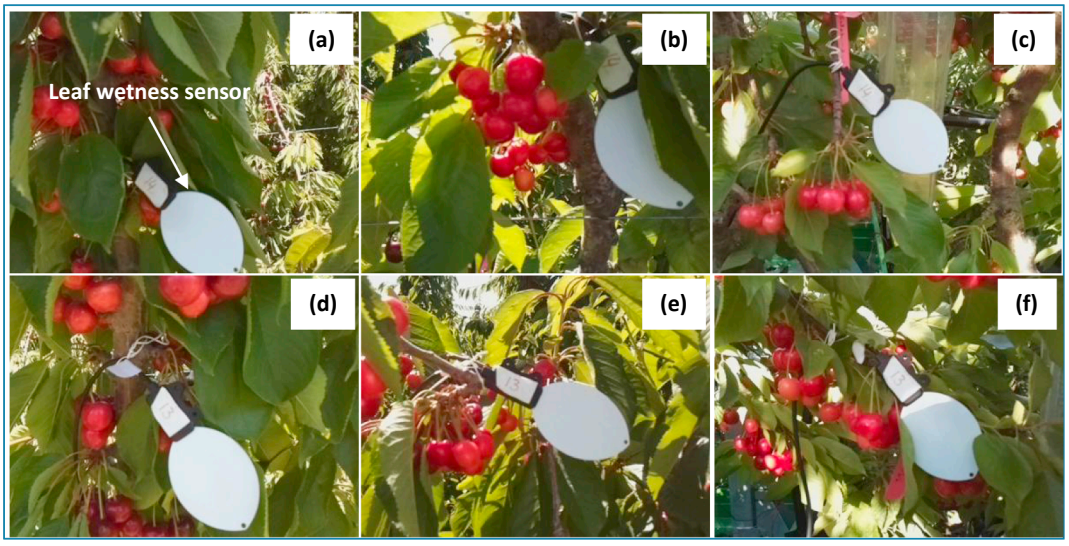

Fig. 2. Sample areas for imaging in two cherry verities of Skeena (a, b, d, e), Selah (c, f).

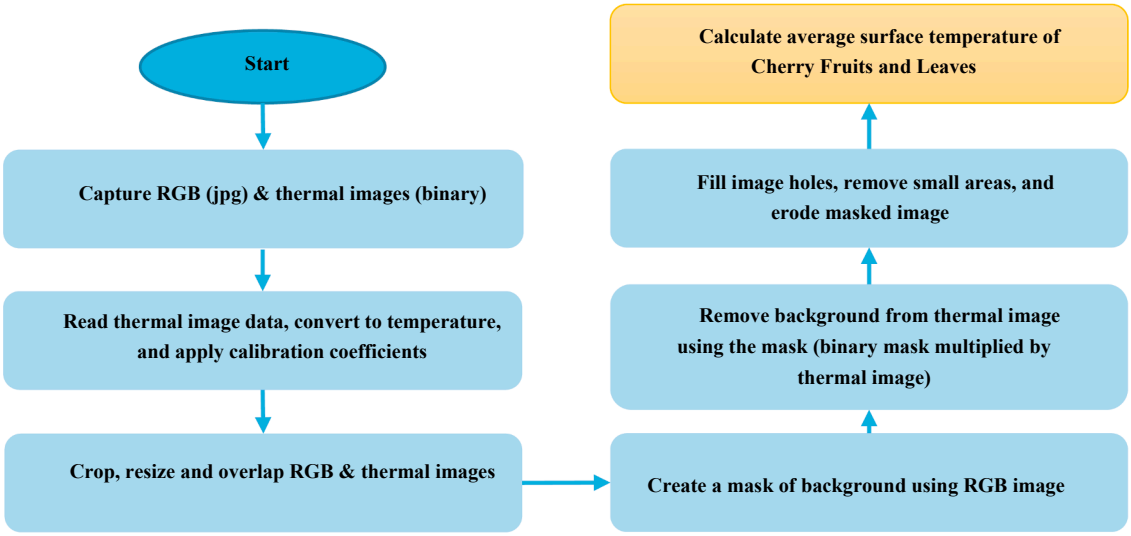

Fig. 3. Flowchart of the image-processing and computer vision algorithm. The algorithm takes RGB and thermal images, creates binary mask and multiplies it by thermal binary image. The resulting image is used to calculate the average surface temperature of cherry leaves and fruits.

actual temperature using a factory conversion equation ($temperature\ (°C) = \frac{Pixel\ \ Value}{100} - 273.15$). Thermal module calibration coefficients determined in the lab were also applied to individual raw pixel values. The cherry binary mask was created by removing the background (i.e. everything else) from RGB images. The background was then removed from thermal images by multiplying the mask by the corresponding thermal image and the average fruit surface temperature was calculated. A similar procedure was carried out to create a binary mask for leaves and calculate the leaf surface temperature. The process of creating masks involved separating the red, green and blue bands of an image using logical indexing, removing small areas, filling holes, and eroding. The bands were compared to segment the image into background and cherries or leaves. The brightness intensity was the basis for distinguishing reflection of cherries on leaves from actual cherries.

The extracted cherry and leaf surface temperature data were compared for a possible relationship. The extracted cherry surface temperature data was used to detect wetness level. To relate the cherry surface temperature to wetness, raw cherry surface temperatures, and surface cherry and air temperature differences were normalized using the following equations, respectively:

$$NRTI = \frac{T_{rt} - T_{min}}{T_{Max} - T_{min}} \quad (1)$$

where $NRTI$ is the normalized raw temperature index, T_{rt} is the real-time cherry surface temperature, T_{min} is the minimum cherry surface temperature right after rain, and T_{Max} is the maximum cherry surface temperature right before rain.

$$NTDI = \frac{\Delta T_{rt} - \Delta T_{Max}}{\Delta T_{Max} - \Delta T_{min}} \quad (2)$$

where $NTDI$ is the normalized temperature difference index, ΔT_{rt} is the difference between air temperature (T_a) and cherry surface temperature (T_{rt}). ΔT_{Max} is the difference between maximum air and cherry surface temperatures ($T_a - T_{rt}$) right after rain. ΔT_{min} is the difference between minimum air and cherry surface temperatures right before rain.

Thermal modules were calibrated based on the following linear equation:

$$T_{tm} = S \times T_{bb} + I \quad (3)$$

where T_{tm} is the surface temperature reading from a thermal-RGB imager, S is the slope of the line (calibration curve), T_{bb} is the temperature of the blackbody calibrator, and I is the intercept of the line.

Other statistical means used here were (a) the root mean square error ($RMSE$), and (b) the mean absolute error (MAE). $RMSE$ and MAE were used as measures of the variance between n thermal module (T_{Lep}) and blackbody calibrator (T_{bb}) measurements:

$$RMSE = \sqrt{\frac{\sum (T_{Lep} - T_{bb})^2}{n}} \quad (4)$$

$$MAE = \frac{\sum |T_{Lep} - T_{bb}|}{n} \quad (5)$$

3. Results and discussion

3.1. Lab calibration of thermal-RBG imaging modules

The thermal-RGB imager calibration results are listed in Table 1. It can be seen that the coefficient of determination was high ($R^2 > 0.999$), and the RMSE, and MAE after calibration were small ($RMSE < 0.6$; $MAE < 0.5$). The results indicated that the measurements were free of outliers ($RMSE \approx MAE$). The average error of thermal modules without calibration was ± 1.7 °C. The highest error reached was ± 2.1 °C which was about half the value reported by the manufacturer (± 5 °C).

3.2. Microclimate during the field trials

Fig. 4 illustrates the fluctuations of air temperature, wind speed, and relative humidity recorded by the microclimate sensing unit in the vicinity of the cherry trees. The air temperature shows temporary drops in the afternoon hours when it is expected to have an increasing trend. This could be clearly related to the cooling effect of evaporation after a simulated rain event as depicted in Fig. 5. Wind speed and relative humidity fluctuation for the course of the experiment are plotted in

Table 1
Linear calibration of thermal modules against the blackbody calibrator.

Module	Before calibration		After calibration				
	RMSE	MAE	RMSE	MAE	Slope	Intercept	R^2
1	1.2	1.2	0.6	0.5	1.0531	−0.6249	0.9989
2	2.1	1.8	0.3	0.2	1.0833	−3.8876	0.9997
Mean	1.7	1.5	0.5	0.4	1.0682	−2.25625	0.9993

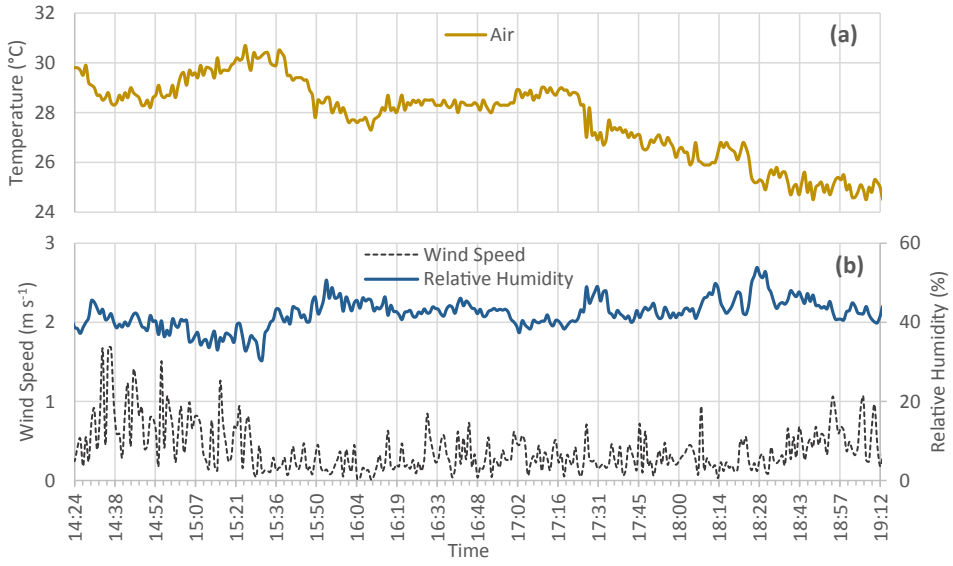

Fig. 4. Plots of microclimate variables during the experiment: air temperature (a), and relative humidity and wind velocity (b).

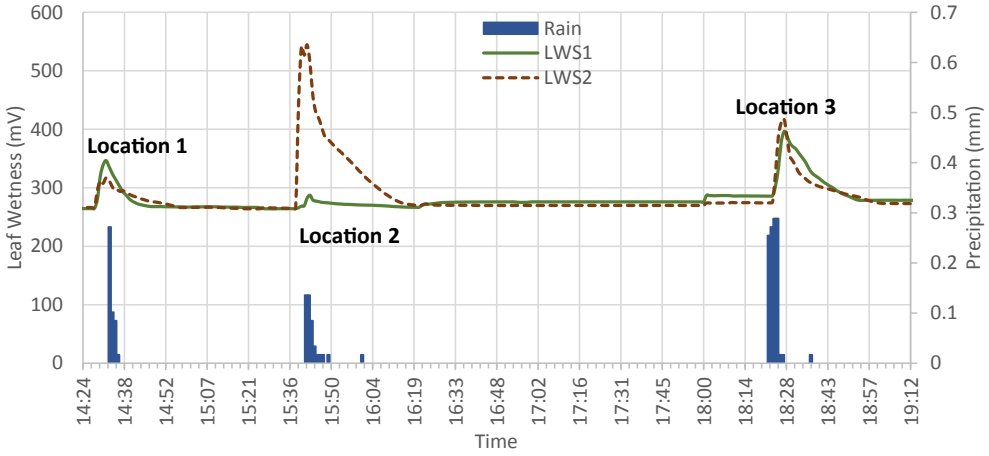

Fig. 5. Canopy wetness monitoring using leaf wetness sensors. The rain depth displayed here was measured using the electronic microclimate measuring unit installed in the vicinity of cherry canopies. Most of the simulated rain was intercepted by the canopies, which significantly reduced the recorded amount of rain.

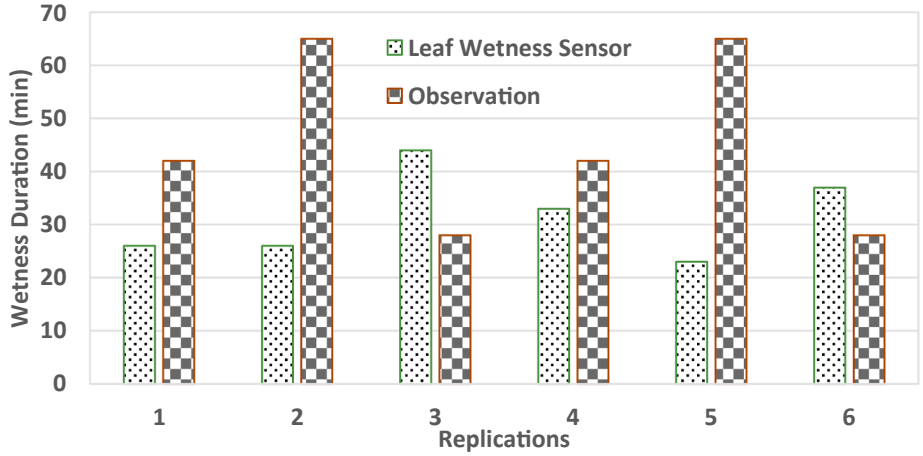

Fig. 6. Comparison between time required for cherries to dry (wetness duration), measured through observation and by leaf wetness sensor for six replications.

Fig. 4b. The relative humidity was varied between 30% and 60%, and wind speed between 0 and 2 ms^{-1}. The relative humidity of the surrounding air did not appear to be affected by the temporary increase in the evaporation rate.

3.3. Measured and observed leaf wetness

The actual amount of rain recorded by the rain gauges (mean) was 2.1, 5, and 2.3 mm for locations 1–3, respectively. The amount of rain

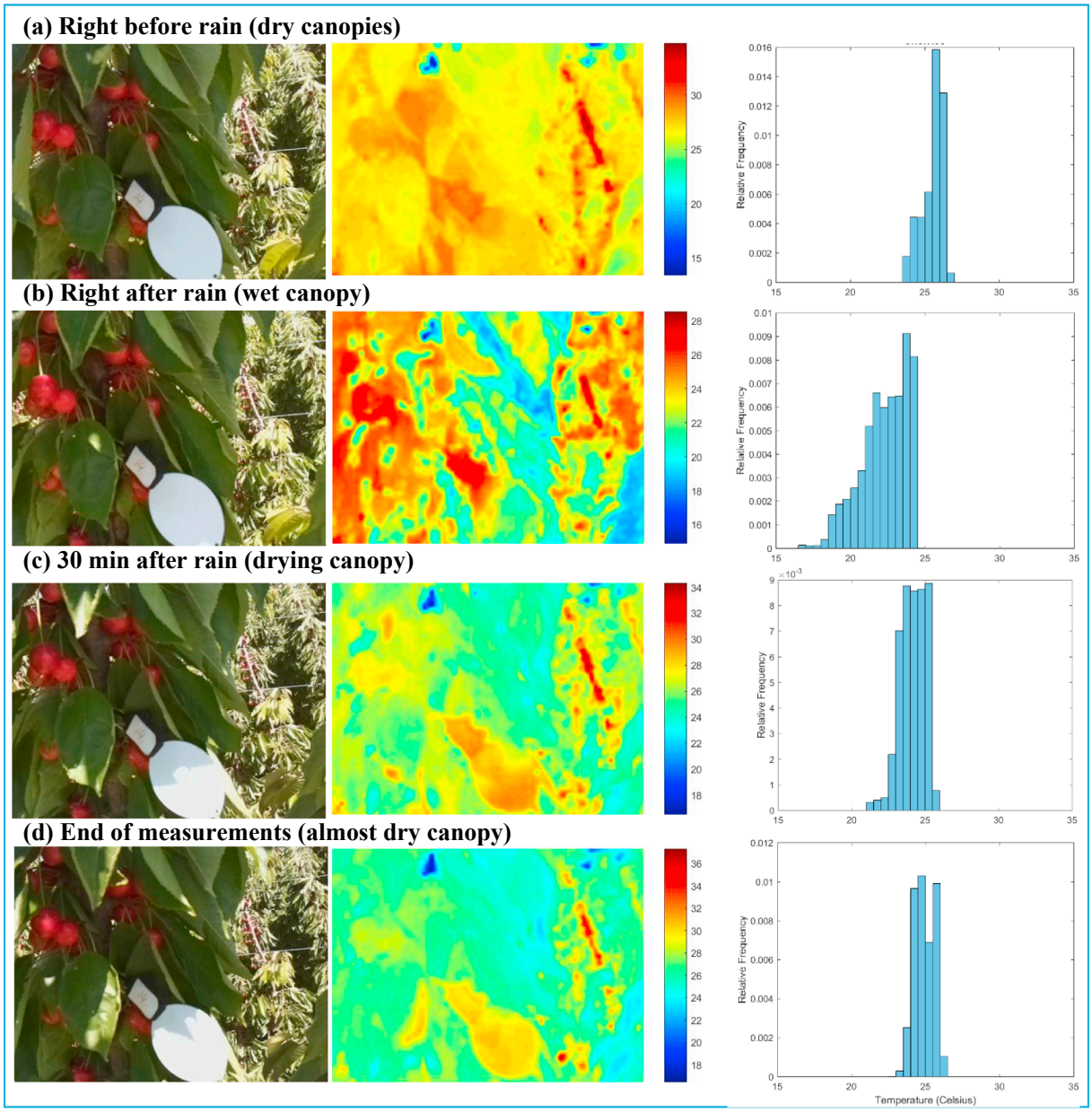

Fig. 7. Sample RGB (left) and thermal images (middle) of sweet cherry canopies captured: right before rain (dry canopies) (a), right after rain (wet canopies) (b), 30 min after rain (drying canopies) (c), and at the end of measurements (almost dry canopies) (d). The relative frequency histogram of surface temperature for the cherry fruits is presented in the right. The rain simulator only affected the cherries and leaves close to the imager. The vertical color bar (middle) shows temperature (°C).

detected by the microclimate sensing unit embedded electronic rain gauge is depicted in Fig. 5 for the three locations. The values are considerably less than the amount applied as most of the rain was intercepted by the cherry canopies. The output signal of the LWS (in mV) is also plotted in Fig. 5. It can be seen that with every rain event, the voltage signal jumped up and then gradually returned to the original value. Both LWSs detected the same wetness period but not the same wetness level, as the intercepted rainwater and consequently the voltage peaks were different.

Fig. 6 depicts the times observed (obtained from direct visual inspection of canopies) for cherries to dry after a simulated rain event, and for LWS to show dry status. As it can be seen, the times are significantly different for these two methods. Further analysis revealed that there was no statistically significant relationship between wetness durations measured by the LWSs and those of measured by observation (result not shown). It is clear that the thermal characteristics, shape and size of the LWS is different from that of surrounding cherries. Consequently, the LWS dried at a different rate.

3.4. Analysis of cherry surface temperatures extracted from thermal images

Sample thermal and RGB images captured by an imager before and after processing are illustrated in Fig. 7. As discussed, RGB images were used to identify cherries and create masks for thermal images. The images in Fig. 7 are representing a dry canopy right before a simulated rain event (Fig. 7a), wet canopy right after the rain (Fig. 7b), drying canopy 30 min after the rain (Fig. 7c), and canopy at the end of the measurement run (Fig. 7d). The relative frequency histograms of cherry fruits in Fig. 7 clearly demonstrates the effect of wetness on temperature distribution. As depicted, the fruit surface temperature of cherries changes over time until the canopy regains its original temperature distribution after it is dried out. This suggests that the temperature

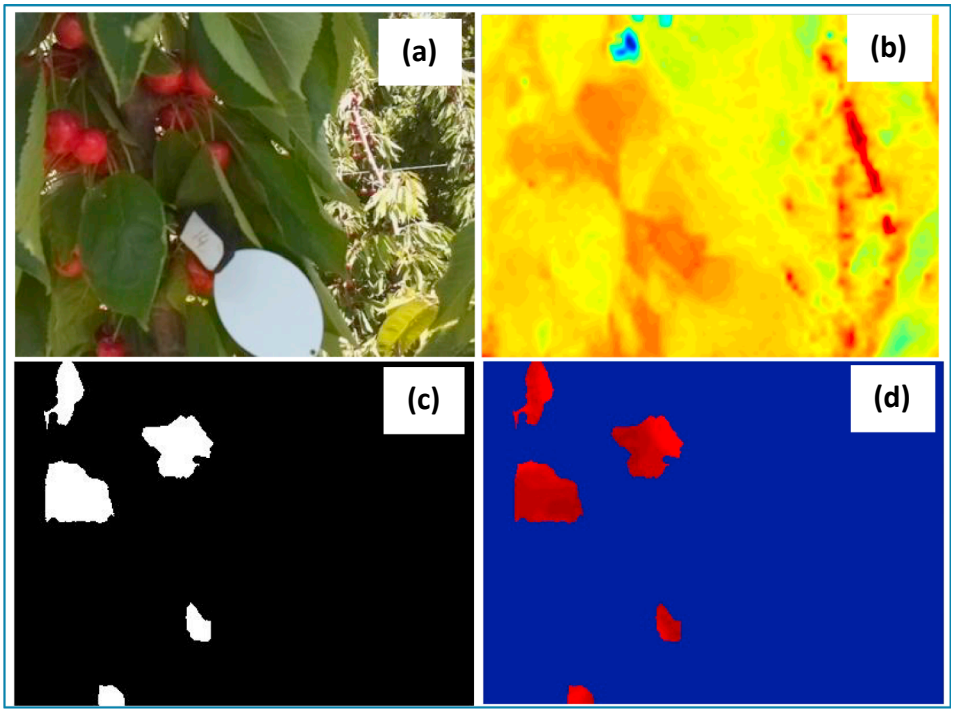

Fig. 8. Sample thermal and RGB images captured by imager, and images as the result of the processing: RGB image (a), thermal false color image (b), binary mask for cherries (c), and thermal image multiplied by the binary mask (d).

variations could be related to wetness level and duration.

About 500 thermal and RGB images were automatically processed using the custom algorithm developed in MATLAB®, and extracted cherry and leaf surface temperatures were exported to an Excel file for further processing. The algorithm was able to effectively separate the cherry target from the background and calculate the surface temperature. Fig. 8 illustrates a sample pair of RGB and thermal images, and generated binary mask and thermal image with background removed. A similar algorithm was used to extract the surface temperature of leaves (images not shown).

Initially the usefulness of raw surface temperatures was investigated towards detecting wetness duration and presence. The results for the six replications are depicted in Fig. 9a. A significant temperature drop of up to 6 °C was observed right after simulated rain event. Overall, the surface temperature of cherries returned to the initial stage (i.e. dry) when the canopies were visually inspected to be dry. Fruit and air temperature difference as an indicator of wetness for the same plots was also investigated. The results are illustrated in Fig. 9b. As it can be seen, air and cherry surface temperature difference significantly increased after wetting canopies during the field experiments.

In order to be able to use cherry surface temperature reading as an indicator of wetness level, we normalized the data according to Eqs. (1) and (2). The maximum possible fruit surface temperature (raw or difference with air temperature) drop (base value) is calculated at the beginning as the difference between the surface temperature (raw or difference with air temperature) before and after simulated rain event. The cherry surface temperature (or its difference with air temperature) is then monitored and its difference with the base value (minimum surface temperature after rain event or maximum difference with air temperature) is calculated continually. Normalized values change between zero and one (or greater than one due to calculation or measurement inaccuracies) with zero indicating 100% wet cherries and one corresponding with a 100% dry cherries. The results are depicted in Fig. 10. The graphs show time to reach different levels of dryness after rain has been applied using the simulator.

3.5. Correlation of cherries and leaves surface temperature

The surface temperature of cherry fruit, as a non-transpiring component of the canopy, was initially higher than that of the leaves. However, both reached the same temperature after a simulated rainfall event. This is shown in Fig. 11 by plotting the liner regression between the two parameters. The surface temperature of the cherries was highly correlated with that of leaves ($R^2 > 0.89$) in all replications. This high correlation suggests that leaf surface temperature could be used as a proxy for cherry surface wetness. This finding can simplify the image processing and computer vision algorithms, and may allow for using stationary infrared thermometers instead of thermal imagers. The correlation appears to be affected negatively if cherries and leaves do not share the same sunlit or shaded fractions. Cherries exposed to the sun will have a higher temperature than the surrounding air, while leaves will have a lower temperature under the same exposure provided they are not water stressed. A larger sample area or averaging values from different locations can mitigate the issue with degree of exposure to the sun. The above finding warrants additional investigation considering the canopies of different age groups under production management.

4. Conclusion

In this effort, the possibility of using a low-resolution thermal-RGB imagery-based system for monitoring the surface temperature of sweet cherry fruits and quantifying the wetness level and duration was assessed. The system relied on inexpensive revolutionary thermal and RGB camera modules. An algorithm was developed to extract the surface temperature of cherries from thermal images. Such systems were deployed in a cherry orchard and a rain simulator was used to apply water and wet the cherry canopies. The results showed that thermal-RGB imagery could be used as a surrogate for traditional wetness monitoring using leaf wetness sensors. Normalized temperature indices (i.e. NTDI and NRTI) were also developed and used to quantify surface wetness level of fruit. A value of '0' indicated a fully wet surface, and a

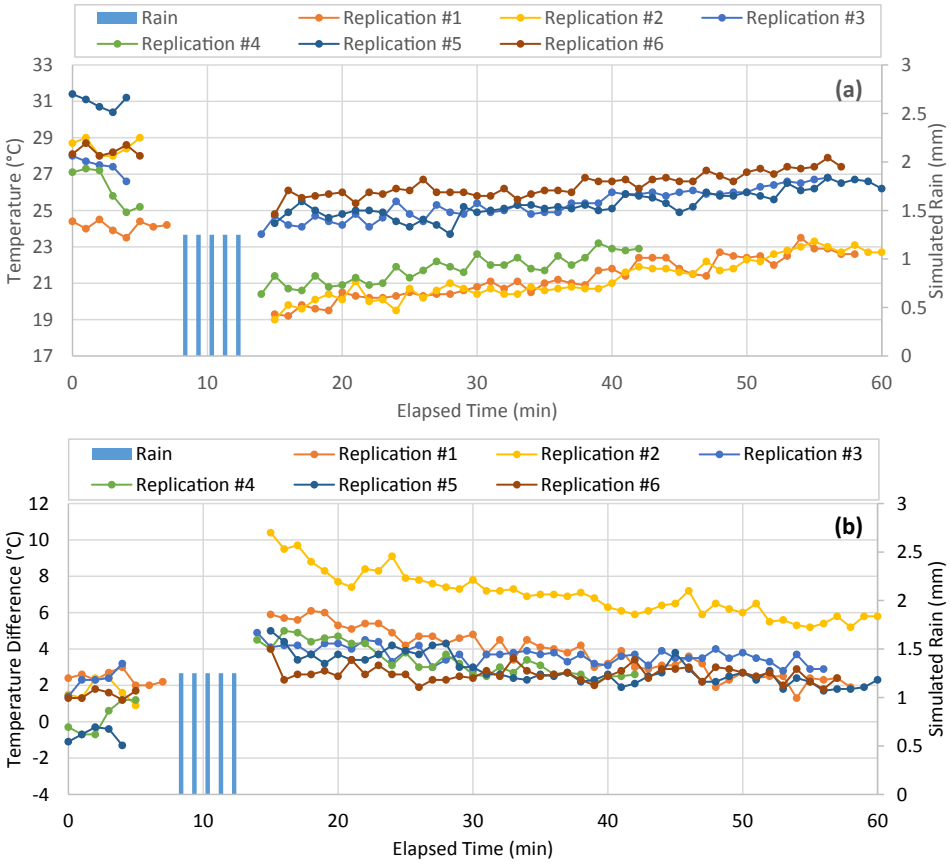

Fig. 9. Plots of raw cherry surface temperature data (a), and air and cherry surface temperature difference (b), for six replications.

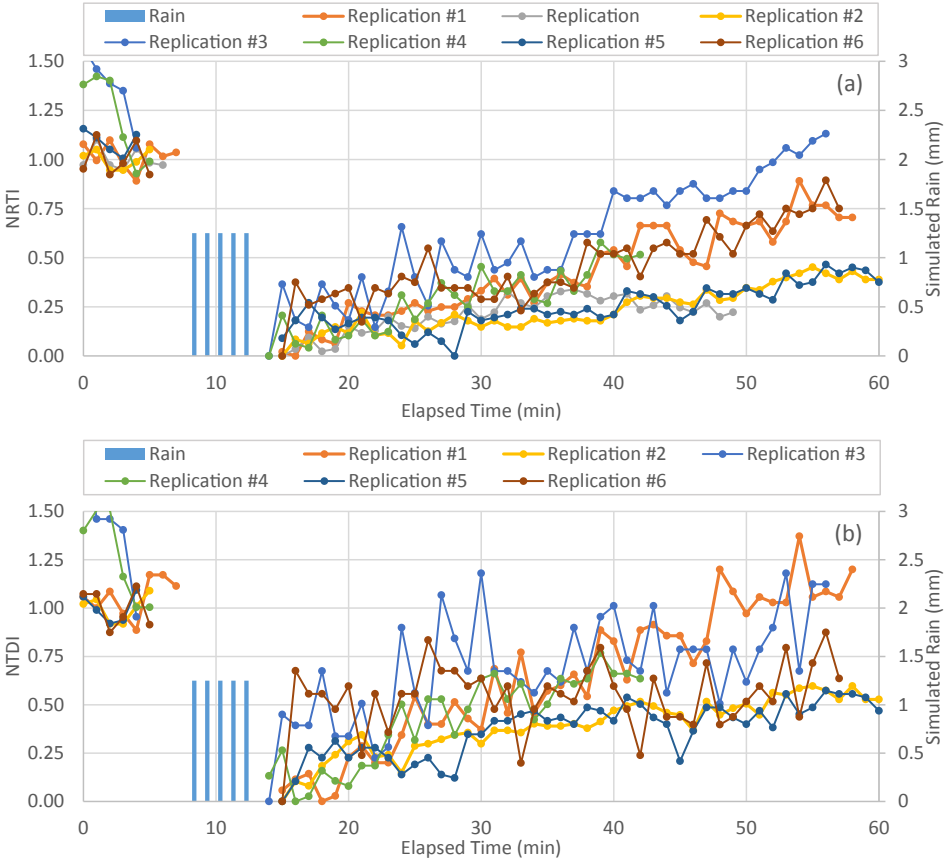

Fig. 10. Plots of normalized cherry surface temperature data (a), and normalized air and cherry surface temperature difference (b), for six replications.

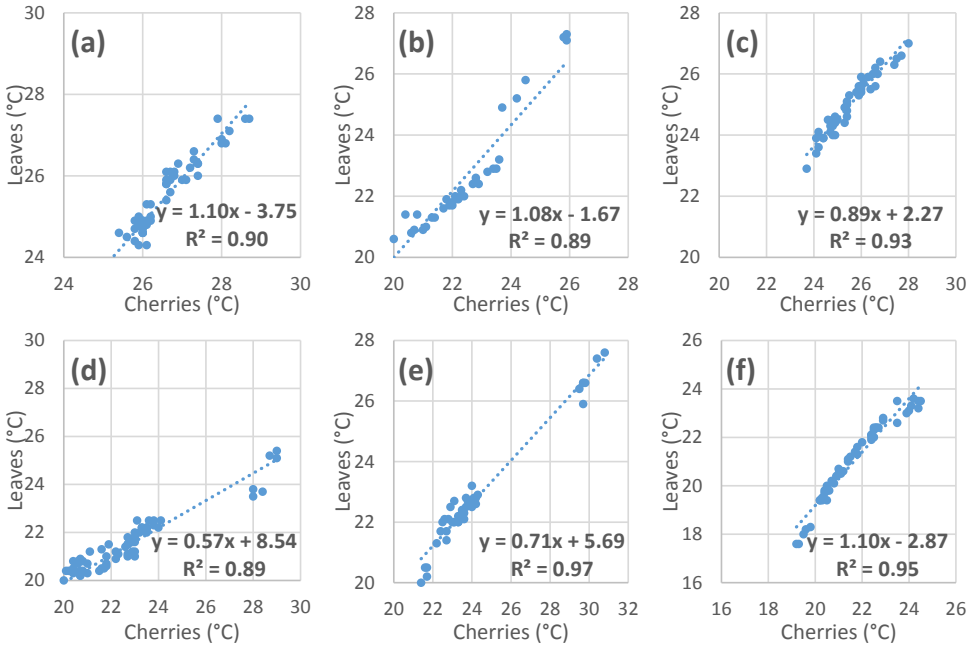

Fig. 11. Plots of linear relationship between the surface temperatures of cherries and leaves for six replications.

value of '1' a fully dried one.

One source of error in our method is surface temperature change simply driven by a change in the sun angle and the percentage of sunlit/shaded cherries in the image rather than wetness. It may cause an increase or decrease in the surface temperature independent of surface wetness. The error could be significant if measurements are taken during daylight hours or days with passing clouds, or days when it is not windy and cherries take more than an hour to dry. To account for this, the computer vision algorithm needs to be able to detect shaded and sunlit cherries/leaves, and calculate the surface temperature and follow the trend separately.

Such monitoring system can be used for tree-fruit surface temperature and wetness monitoring for effective actuation of management methods. The measurements can be integrated into a wireless sensor network to collect information on both spatial and temporal variations of wetness in orchards. By utilizing the proposed imagery-based system, fruit cracking mechanism may be fully understood, and decision aid tools may be developed for efficient rainwater removing to prevent fruit cracking.

Acknowledgements

The authors would like to thank Dr. Matthew Whiting, Mr. Rajeev R. Sinha, Mr. Haitham Y. Bahlol, and Mr. Chongyuan Zhang, Washington State University for their help in the completion of this study. The authors would also like to thank Dr. Lav Khot, Washington State University for his help with editing the manuscript draft and facilitating the experiments. The authors also acknowledge the assistance, funding and support from the Center for Precision and Automated Agricultural Systems (CPAAS) at Washington State University.

References

Chandel, A.K., Khot, L., Osroosh, Y., Peters, R.T., 2018. Thermal-RGB imager derived in-field apple surface temperature estimates for sunburn management. Agric. For. Meteorol. 253–254, 132–140.

Cosh, M.H., Kabela, E.D., Hornbuckle, B., Gleason, M.L., Jackson, T.J., Prueger, J.H., 2009. Observations of dew amount using in situ and satellite measurements in an agricultural landscape. Agric. For. Meteorol. 149 (6–7), 1082–1086.

Duttweiler, K.B., Gleason, M., Dixon, P.M., Sutton, T.B., McManus, P.S., Monteiro, J.E.B., 2008. Adaptation of an apple sooty blotch and flyspeck warning system for the Upper Midwest United States. Plant Dis. 92, 1215–1222.

Hatfield, J., 1982. Biometeorology in Integrated Pest Management, first ed. Elsevier Inc., pp. 502.

Heusinkveld, B.G., Berkowicz, S.M., Jacobs, A.F.G., Hillen, W., Holtslag, A.A.M., 2008. A new remote optical wetness sensor and its applications. Agric. For. Meteorol. 148 (4), 580–591.

Hornbuckle, B.K., England, A.W., Anderson, M.C., Viner, B.J., 2006. The effect of free water in a maize canopy on a microwave emission at 1.4 GHz. Agric. For. Meteorol. 138, 180–191.

Kafle, G.K., Khot, L.R., Zhou, J., Bahlol, H.Y., 2016. Towards precision spray applications to prevent rain-induced sweet cherry cracking: understanding calcium washout due to rain and fruit cracking susceptibility. Sci. Hortic. 203, 152e157.

Khanal, S., Fulton, J., Shearer, S., 2017. An overview of current and potential applications of thermal remote sensing in precision agriculture. Comput. Electron. Agric. 139, 22–32.

Llorente, I., Vilardell, P., Bugiani, R., Gerardi, I., Montesinos, E., 2000. Evaluation of BSPcast disease-warning system in reduced fungicide use programs for management of brown spot of pear. Plant Dis. 84, 631–637.

Mahlein, A.-K., Oerke, E.-C., Steiner, U., Dehne, H.-W., 2012. Recent advances in sensing plant diseases for precision crop protection. Eur. J. Plant Pathol. 133, 197–209.

Osroosh, Y., Khot, L., Peters, R.T., 2018. Economical thermal-RGB imaging system for monitoring agricultural crops. Comput. Electron. Agric. 147, 34–43.

Peres, N.A., Timmer, L.W., 2006. Evaluation of the Alter-Rater model for spray timing for control of Alternaria brown spot of Murcott tangor in Brazil. Crop Prot. 25, 454–460.

Pinter Jr., P.J., 1986. Effect of dew on canopy reflectance and temperature. Remote Sens. Environ. 19 (2), 187–205.

Ramalingam, N., Ling, P.P., Derksen, R.C., 2004. Field Evaluation of Ground based Multispectral Imaging Techniques for Leaf Surface Wetness Sensing. ASABE Paper No. 043063. Ottawa, Ontario, Canada.

Rowlandson, T., Gleason, M., Sentelhas, P., Gillespie, T., Thomas, C., Hornbuckle, B., 2015. Reconsidering leaf wetness duration determination for plant disease management. Plant Dis. 99 (3), 310–319.

Sankaran, S., Mishra, A., Ehsani, R., Davis, C., 2010. A review of advanced techniques for detecting plant diseases. Comput. Electron. Agric. 72, 1–13.

Sentelhas, P.C., Gillespie, T.J., Santos, E.A., 2007. Leaf wetness duration measurement: comparison of cylindrical and flat plate sensors under different field conditions. Int. J. Biometeorol. 51, 265–273.

Sutton, J.C., Gillespie, T.J., Hildebrand, P.D., 1984. Monitoring weather factors in relation to plant disease. Plant Dis. 68, 78–84.

Zhou, J., Khot, L.R., Bahlol, H.Y., Kafle, G.K., Peters, T., Whiting, M.D., Zhang, Q., Granatstein, D., Coffey, T., 2017. In-field sensing for crop protection: efficacy of air-blast sprayer generated crosswind in rainwater removal from cherry canopies. Crop Prot. 91, 27–33.

Zhou, J., Khot, L.R., Peters, T., Whiting, M.D., Zhang, Q., Granatstein, D., 2016. Efficacy of unmanned mid-sized helicopter downwash in rainwater removal from cherry canopies. Comput. Electron. Agric. 124, 161e167.